Acta Acustica 2024, **8**, 15
© The Author(s), Published by EDP Sciences, 2024
https://doi.org/10.1051/aacus/2024007

Topical Issue - Virtual acoustics

Available online at:
https://acta-acustica.edpsciences.org

SCIENTIFIC Article OPEN ACCESS

Wind farm noise prediction and auralization

Andrea P. C. Bresciani[1,2,*], Julien Maillard[1], and Arthur Finez[3]

[1] Centre Scientifique et Technique du Bâtiment (CSTB), 24 Rue Joseph Fourier, Saint-Martin-d'Hères, 38400, France
[2] University of Twente, Drienerlolaan 5, 7522 NB, Enschede, The Netherlands
[3] ENGIE Green, 6 rue Alexander Fleming, 69007, Lyon, France

Received 13 December 2023, Accepted 18 February 2024

Abstract – This work presents the application and validation of a novel auralization approach for the evaluation of wind turbine noise annoyance under diverse conditions. The approach is based on the decomposition of each turbine blade into elementary short-segment sources, whose acoustic radiation in the far field is obtained by coupling Amiet's emission model with the Harmonoise engineering model for outdoor sound propagation. The transfer functions between the elementary source positions and receivers are obtained. Then, the average and instantaneous sound pressure levels are calculated over one blade rotation. The realism of the audio signals is evaluated through listening tests with audio signals of the real and simulated environments. The predicted noise spectra from five wind turbines capture well the measured trends and the absolute levels. Finally, we present a study of the weather effects on noise emissions and propagation by using the numerical model developed.

Keywords: Wind turbine noise, Auralization, Outdoor sound propagation

1 Introduction

The increasing demand for renewable energy has led to a significant rise in wind turbine installations. When it comes to on-shore installations, specific regulations are in place to govern the acoustic impact of wind turbines on nearby residences. These regulations consider factors like the distance between the turbine and the dwelling and the extent to which the noise level exceeds the background noise. These rules are necessary due to the noise-related disturbances caused by wind turbines in certain situations. Research by Janssen et al. [1] revealed that wind turbine noise is perceived as more annoying than other sources such as wind, road, and rail, despite having lower or comparable sound levels. Consequently, wind turbine manufacturers and operators face the challenge of increasing energy production while minimizing noise disturbance and adhering to regulatory standards. Achieving this balance necessitates optimizing the design, placement, and operation of wind turbines.

Regarding noise emission, the optimization process would significantly benefit from simulation tools that can precisely predict noise levels emitted by wind turbines under specific circumstances. Consequently, extensive research has been conducted in recent years to create and enhance these simulation tools [2–8]. Additionally, there has been a growing need to auralize wind turbine noise to facilitate the exploration and comprehension of noise annoyance mechanisms. Auralization, in this context, enables the evaluation of wind turbine noise annoyance under diverse conditions through auditory tests. These tools might also prove valuable in promoting the acceptance of wind turbines by illustrating their acoustic impact through augmented reality applications founded on accurate auralized soundscapes.

Previous work on the auralization of wind turbine noise includes sampled-based auralization and physics-based auralization. Pieren et al. [9] proposed a sample-based methodology where recorded samples are used to obtain the parameters of the synthesized signal, which includes a tonal component and an amplitude-modulated broadband part. Results from listening tests comparing actual audio recordings with synthetic signals indicated an acceptable level of realism. This type of approach is however limited by the restricted number of modeled scenarios imposed by the conditions of the recording. On the other hand, physics-based auralization uses a numerical model whose parameters may be freely adjusted to address a wider range of configurations. This is the approach adopted in the present work. It requires modeling first the aerodynamic noise emission of the wind turbine, which is the dominant noise source, and second, its propagation to the receiver. The frequency and time-dependent characteristics of the noise emission and atmospheric propagation models are then applied to appropriate signal processing algorithms to construct a spatialized 3D audio signal at the receiver location.

The display of Audio files embedded in this PDF depends on the software used (PDF reader, video player, installed codec, direct display in the browser, etc.). Please see the Adobe Acrobat page for more explanation.

* Corresponding author: andrea.bresciani@vki.ac.be

This is an Open Access article distributed under the terms of the Creative Commons Attribution License (https://creativecommons.org/licenses/by/4.0), which permits unrestricted use, distribution, and reproduction in any medium, provided the original work is properly cited.

A cost-efficient modeling approach for the source emission is based on Amiet's theory [10, 11]. This model can then be coupled with ray-tracing or parabolic equation methods to obtain the noise levels in the far field, taking into account ground and atmospheric propagation effects. Recently, Mascarenhas et al. [12] and Mascarenhas [13] developed a physics-based approach for the auralization of wind turbine noise. The approach is based on the decomposition of each turbine blade into elementary short-segment sources, whose acoustic radiation in the far field is obtained by coupling Amiet's emission model with the parabolic equation [2]. Short-time signals associated with different blade segments at different angular positions are then calculated based on the radiated sound pressure level at the receiver location. These short-time signals are finally cross-faded using an appropriate window function to construct the signal for a complete blade rotation.

Unlike the method above, the approach used in the present work employs a continuous-time signal, which is amplitude-modulated and delayed based on the time-dependent noise levels computed for discrete blade segment positions. As a result, the method allows for a continuous time-varying delay, thus properly rendering Doppler shifts. Another advantage of the method is to decouple the calculation of the emission source signals from the far-field propagation effect rendering. This facilitates integrating the method in previously developed auralization systems [14–16] to combine wind turbine sources with other noise sources such as road or railway traffic noise. The wind turbine blade is decomposed in a set of short blade segments where the acoustic radiation of each segment is modeled by a single aerodynamic elementary source. This source power and directivity is computed using a RANS-based Amiet's theory for leading- and trailing-edge noise [10, 11]. Figure 1 shows qualitatively the typical relative importance of leading- and trailing-edge noise to the total noise spectrum in modern large wind turbines. While trailing-edge noise is the dominant noise source at high frequencies, leading-edge noise becomes more important at low frequencies and, particularly, in a highly turbulent environment. The contribution of each elementary source to the receiver located in the far field is then calculated using engineering ray-based methods for outdoor sound propagation. Compared to the parabolic equation or standard ray tracing in refracting medium, these engineering models have a much lower computational cost while still providing an accuracy of ±3 dB at distances commonly encountered for wind turbine sound propagation. This accuracy is usually acceptable for environmental noise propagation studies. The approach can therefore be applied to wind farms with multiple wind turbines in complex environments including topography, buildings, and other noise sources. In this work, the Harmonoise model proposed by Salomons et al. [17] and van Maercke and Defrance [18] is implemented as it includes a more refined meteorological model considering refraction due to specific wind conditions and turbulence scattering effects.

The overall process includes two distinct steps. First, the blade segment emission characteristics are computed for several blade geometries and operating conditions such as wind and rotational speed. Second, the transfer functions between elementary blade source positions and receivers are obtained, followed by the averaged sound pressure levels over one blade rotation and the auralized audio samples using the emission characteristics database. Note that this second phase has been integrated into CSTB's outdoor noise auralization software, .

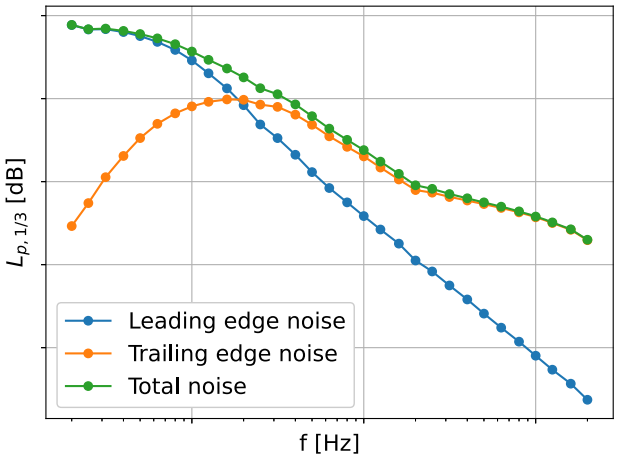


Figure 1. Contributions of leading- and trailing-edge noise to the total 1/3-octave band noise levels of a modern large wind turbine.

The present work describes the results of the validation of the approach against on-site measurements of operating wind turbines. The measurements have been provided by Engie Green and obtained from a private research project conducted in collaboration with UMRAE [19]. The validation consists of first comparing the measured sound pressure levels at different locations around the wind turbines with those obtained at the same locations with the proposed approach. Second, the realism of the auralized signals is evaluated through listening tests mixing recorded audio signals of the real environments and auralized signals of the simulated environment.

The outline of the paper is as follows. Section 2 presents the measurement site and recorded audio samples. Section 3 describes the modeling of the site and the generation of auralized audio samples. Section 4 compares the predicted and measured noise spectra and the realism of the auralized noise signals. Some of the results included in this section have been presented in reference [20]. Finally, Section 5 presents a study of the influence of weather conditions on sound emission and propagation. The conclusions of this work are summarized in Section 6.

2 Measurement site

The measured data was collected on an existing site, equipped with five 2 MW wind turbines of rotor diameter, 92 m, and hub height, 100 m. The terrain can be considered flat with cultivated fields of the same type. Acoustic measurements used Class 1 sound level meters positioned at various locations, upwind, downwind, and in the crosswind



Figure 2. View of one of the measurement points upwind of the wind turbine. The microphone is placed on a hard 1 m diameter board and protected by a windscreen according to IEC 61400 specifications.

directions of the wind turbines, with distances from 150 m, i.e. close to the machines, according to the IEC 61400 standard specifications, up to 1.5km. Measured data includes continuous 1/3-octave band equivalent levels between 12.5 Hz and 20 kHz with a 1 s integration constant. In parallel, the measured sound pressure signal was recorded at a 25.6 kHz sampling frequency for listening tests and additional frequency analysis. The selected sampling frequency is sufficiently high to capture the frequency content of interest, specifically up to the 1/3-octave band with a central frequency of 10 kHz. Typically, higher frequencies are not relevant for atmospheric propagation of wind turbine noise as atmospheric absorption considerably attenuates noise above 10 kHz. Additionally, the frequency content of wind turbine noise sources is usually very low above this frequency. Hence, the background noise levels are usually higher than the wind turbine noise above 10 kHz after a few hundred meters, owing to these two reasons. Simultaneous meteorological data was measured using a LiDAR system, six 3D sonic anemometers, and a 100 m mast equipped with several anemometers, thermometers, and one hygrometer. Finally, wind turbine operation data were also collected including rotational speed, blade pitch angle, wind speed, and wind direction at hub height. Figure 2 shows a view of one of the IEC 61400 measurement points upwind of the wind turbine.

The results presented in this work include two sets of wind turbine Operating Conditions (OC), referred to as

Table 1. Positions of the turbines (WT1 to WT5), microphones close to WT1 (SB1 to SB3), and far-field microphones downwind (P1 to P9) and upwind (C1 to C5).

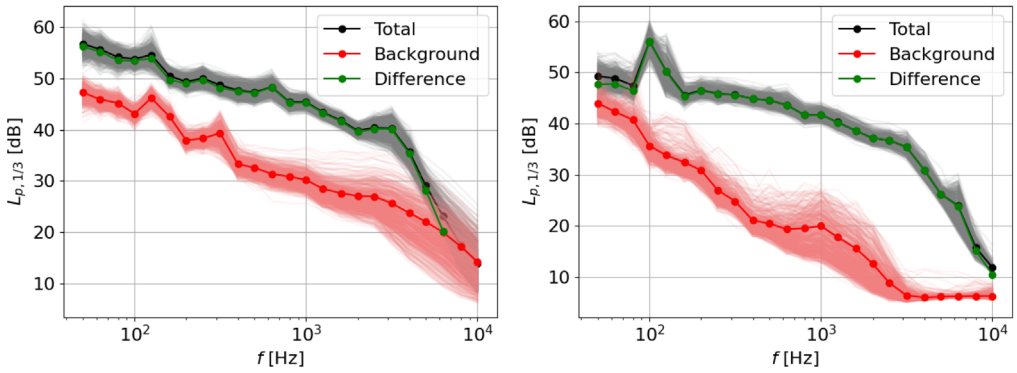
	x (East) [m]	y (North) [m]	Hub/Receiver height [m]
WT1	753.7	1071.0	100
WT2	941.9	867.0	100
WT3	1107.9	644.0	100
WT4	1223.7	396.0	100
WT5	1288.4	134.0	100
SB1	884.9	1153.7	0
SB2	677.2	1200.1	0
SB3	620.6	1011.9	0
P1	1363.6	815.7	1.5
P6	1940.7	1065.1	1.5
P8	2247.4	1170.8	1.5
P9	2511.4	1329.4	1.5
C1	824.8	542.9	1.45
C3	656.1	460.2	1.73
C5	425.4	346.7	1.7

Table 2. Operating Conditions (OC) simulated. If available, the standard deviation σ_m is given after the time average μ_m as $\mu_m \pm \sigma_m$.

	OC1	OC2
Rotor speed [rpm]	15.10 ± 0.093	13.72 ± 0.15
Pitch angle [°]	7.8 ± 1.1	0.0 ± 0
Wind speed at 100 m [m/s]	12.2	7.54
Wind speed at 10 m [m/s]	8.3	5.1
Wind orientation [°]	220 ± 2.4	259 ± 1.5
Turbulence intensity [%]	13.0 ± 2.7	7.75 ± 1.2
Turbulence length scale [m]	300	300
Humidity [%]	86	98
Temperature [°C]	5	8
Nebulosity [okta]	2	8
Time	Night	Night
Time average period [min]	18	10

OC1 and OC2, whose parameters are taken from two different time periods during the measurement campaign. The details of the Operating Conditions are listed in Table 2. The wind orientation (wind origin) is measured counterclockwise from the North. During the measurements, the wind turbines were programmed to start and stop at prescribed times. By considering measured data before and after a stop time, the noise levels and associated audio recordings can be obtained for total noise (i.e. including both wind turbine and background noise), and background noise, respectively. The transient periods have not been considered in the recordings and analysis. The measurements were performed at night to benefit from a lower background noise and a better signal-to-noise ratio.

Table 1 gives the exact positions of the microphones and wind turbines. The arbitrary position (0, 0) corresponds to the lower-left corner in Figure 4. A schematic of the wind farm layout and the position of the receivers will be shown in Figure 4. The receivers referred to as SB1, SB2, and SB3, correspond to three IEC measurement points, i.e. at a



(a) SB1, OC1 (b) SB1, OC2

(c) SB2, OC1 (d) SB2, OC2

(e) SB3, OC1 (f) SB3, OC2

Figure 3. Total and background noise spectra at the receiver SB locations. The thin lines represent the 1 s equivalent levels and the thick lines, the overall average levels. The predicted spectra are compared with the difference (computed in Pascal squared) between the total and background levels, i.e. the estimate of the turbine noise only.

150 m distance, for the North wind turbine. The receivers from P1 to P9 and C1 to C5 are respectively downwind and upwind of the wind farm.

Figure 3 presents the total and background noise levels for receiver SB1, SB2, and SB3 for OC1 and OC2. In the spectra of OC2, the 58 dB peak at 100 Hz is attributed to the mechanical noise emitted by the gearbox. The measured noise levels are higher in OC1 and the aerodynamic broadband noise masks the mechanical noise. The tone at 4 kHz measured for SB3 and present in both OCs is probably due to a whistle of the recording system.

The numerical spectra will be compared in Section 4 with the difference (in Pascal squared) $L_{\mathrm{p,turbine}} = 10\log_{10}(S_{\mathrm{pp,total}} - S_{\mathrm{pp,background}})$ between the total, $S_{\mathrm{pp,total}}$ [Pa^2], and background levels, $S_{\mathrm{pp,background}}$ [Pa^2]. Only the values for which $L_{\mathrm{p,turbine}} > L_{\mathrm{p,background}}$ are considered reliable and used for the comparison. Note that this condition corresponds to imposing a signal-to-noise ratio higher than

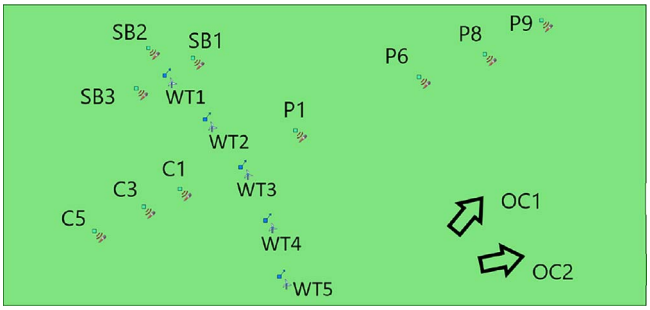


Figure 4. MithraSOUND® 2D view of the modeled site including the five wind turbines and the three receivers SB1, SB2, and SB3. Wind direction for OC1 and OC2 is shown at the bottom right.

3 dB. The resulting levels $L_{\mathrm{p,turbine}}$ are shown, in green, in Figure 3.

3 Wind farm noise predictions and auralized audio samples

The numerical workflow starts from the 3D CAD of the wind turbine blade. As the CAD of the measured wind turbine was not available for this study, the blade of the generic SWT 2.3-93 (2.3 MW rated power and 93 m of diameter) wind turbine [21, 22] is used instead. The two turbines belong to the same class and have similar rated power and diameter. For this reason, the differences in the emitted noise levels are expected to be negligible for the scope of the present study and within the error margins of the numerical approach adopted. The wind turbine blade is decomposed into $N_{\mathrm{seg}} = 6$ blade segments. The methodology is based on a RANS-informed Amiet's model [11] for trailing-edge noise. The mid-span airfoil of each segment is used in a 2D Reynolds-averaged Navier–Stokes (RANS) simulation to compute the boundary layer parameters required by Amiet's theory for trailing-edge noise [23]. Lee's [24] and Goody's [25] empirical models are used to predict the wall pressure spectra for adverse and favorable pressure gradients, respectively. The leading-edge noise is also considered using Amiet's theory [10]. The aeroacoustic transfer functions for the leading- and trailing-edge noise are taken from reference [26]. The turbulence spectrum is used to model the velocity spectrum with a turbulence intensity of 13.0% of the wind speed for OC1 and 7.75% for OC2. The turbulence intensity was measured by the LiDAR system upwind of the turbines at 100 m height. The integral length scale was not measured. A reasonable value for flat terrain and a neutral atmosphere is around 300 m and this value is used in the simulations. It will be shown in Section 5.1 that the noise predictions have a low sensitivity to the integral length scale; hence, an error in this estimate does not greatly influence the predicted levels. For each blade segment, the far-field radiated power and directivity data are computed for both operating conditions, OC1 and OC2.

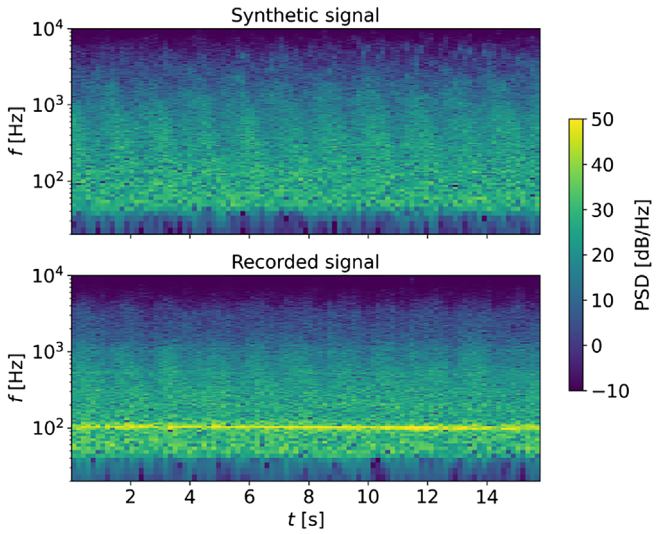


Figure 5. Spectrogram of auralized (top) and recorded (bottom) samples for SB2 and OC2. The spectrogram is obtained with a block size of 8192 samples and a Tukey window with 25% overlap. The sampling frequency of the synthetic and recorded audio signals are 44.1 kHz and 25.6 kHz, respectively.

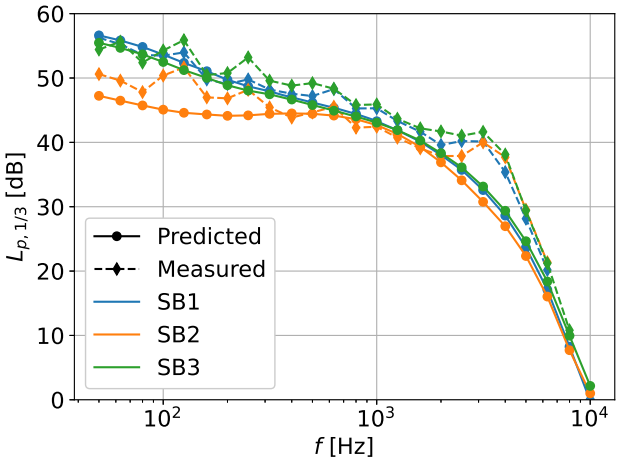
To apply the Harmonoise model (or, in general, any engineering model) to a wind turbine, the rotor disk is discretized in the azimuthal direction in 360 stations, resulting in a total of $360N_{\mathrm{seg}}$ elementary sources. The number of azimuthal stations (i.e. 360) is sufficiently large to avoid inaccuracies due to the discretization. The convective effects included in Amiet's theory are considered by evaluating the directivity and spherical divergence for the blade segment located in the *present source position* [27, 28]. This is necessary because Amiet's theory is formulated in terms of present source coordinates [27]. Instead, the excess attenuation is calculated using the *emission position* as it is independent of the coordinate system in which the source model is derived.

The Harmonoise model calculates the sound pressure levels $\tilde{L}_{p,ik}$ emitted by the elementary source i at the receiver k in 1/3-octave band (from 50 Hz to 10 kHz) as

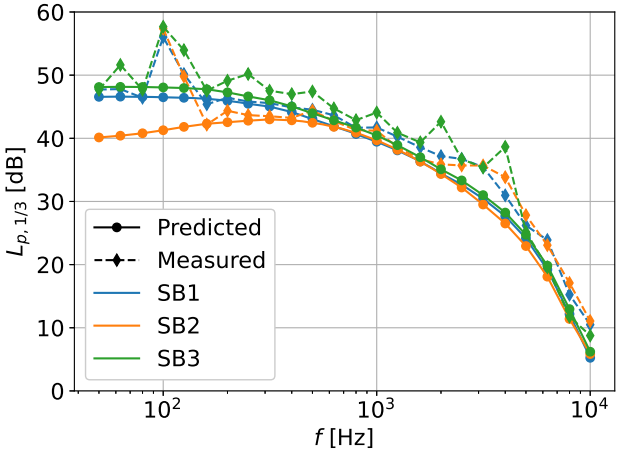
$$\tilde{L}_{p,ik} = L_{w,i} + DI_{ik} - A_{\mathrm{div},ik} - A_{E,ik}, \tag{1}$$

where $L_{w,i}$ and DI_{ik} represent, respectively, the sound power and the directivity of the source i in the direction of the receiver k and they are computed using Amiet's theory. $A_{\mathrm{div},ik}$ denotes the spherical divergence, $A_{E,ik}$ is the excess attenuation that, in this work, includes the effect of the ground reflection, atmospheric refraction, atmospheric absorption, and turbulence scattering. The 1/3-octave noise spectra including the Doppler effect are calculated as explained in reference [28]. These noise levels do not include the Doppler effect yet and are used for the auralization methodology described in reference [29] and briefly recalled here below.

For each segment of each blade, the pressure time signal $\tilde{p}$ (no Doppler effect is considered at this stage) is computed using the spectral shaping synthesis technique as

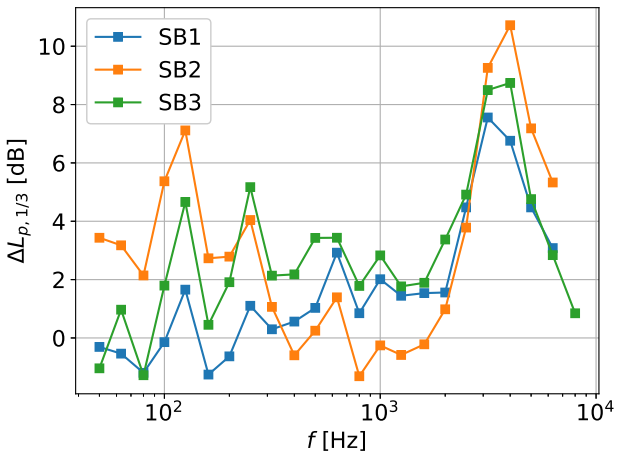


(a)

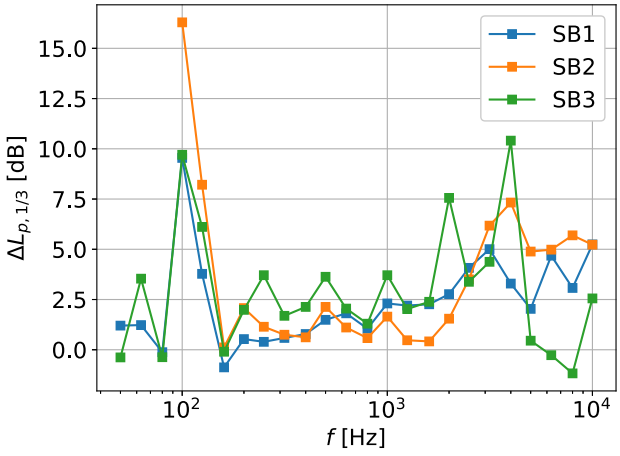


(b)

Figure 6. Comparison of the measured (dashed lines) and predicted (solid lines) 1/3-octave band levels for receivers SB1, SB2, and SB3, and operating conditions (a) OC1 and (b) OC2.



(a)



(b)

Figure 7. Difference between measured and predicted 1/3-octave band levels ($\Delta L_{\mathrm{p,1/3}} = L_{\mathrm{p,1/3,measured}} - L_{\mathrm{p,1/3,predicted}}$) for receivers SB1, SB2, and SB3, and operating conditions (a) OC1 and (b) OC2.

$$\tilde{p}(t) = \sum_{i_f=1}^{N_b} p_{\mathrm{rms},i_f}(t)\frac{n_{i_f}(t)}{n_{\mathrm{rms}}} \tag{2}$$

where N_b is the number of 1/3-octave frequency bands, $n_{i_f}(t)/n_{\mathrm{rms}}$ is the band-filtered normalized pink noise in the 1/3-octave band i_f, and $p_{\mathrm{rms},i_f}(t)$ is the root-mean-square (RMS) amplitude of the signal for the band i_f. The RMS amplitude of the signal is calculated from the sound pressure levels $\tilde{L}_{p,i_f}$[1] as

$$p_{\mathrm{rms},i_f}(t) = p_0\sqrt{10^{\tilde{L}_{p,i_f}(t)/10}} \tag{3}$$

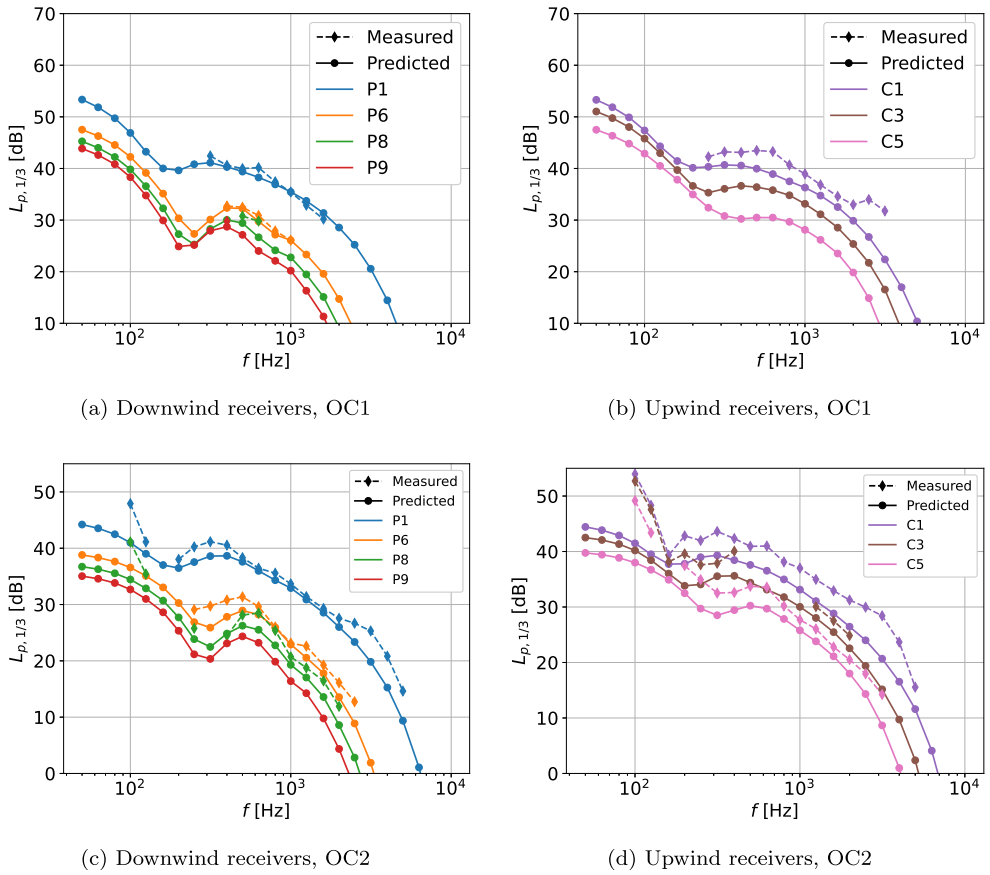
with $p_0 = 2 \times 10^{-5}$ Pa. Finally, the Doppler effect is included in the time domain as a time-varying propagation time $\tau(t)$, i.e.

$$p(t) = \tilde{p}(t - \tau(t)). \tag{4}$$

[1] The subscripts ik are dropped here to simplify the notation.

For the calculation of $\tau(t)$ the reader is referred to reference [29]. The pressure time signal of one blade is obtained by summing the contribution from each segment. The time signal of one blade is delayed by 1/3 and 2/3 of the rotation period to represent the other two blades.

The measurement site is then modeled in Mithra-SOUND®, including the 5 wind turbines and a set of receiver points according to the measurement locations, as shown in Figure 4. The three IEC receiver locations, SB1, SB2, and SB3, are approximately downwind, crosswind, and upwind, respectively, as can be seen from the wind direction of operating conditions OC1 and OC2 also shown in the figure. The meteorological conditions for the numerical simulations were taken from the database of reference [30] at the closest airport. Both conditions correspond to night time with a nebulosity of approximately 2 okta for OC1 and 8 for OC2, a wind speed (10 m above ground)



(a) Downwind receivers, OC1

(b) Upwind receivers, OC1

(c) Downwind receivers, OC2

(d) Upwind receivers, OC2

Figure 8. Comparison of the measured (dashed lines) and predicted (solid lines) 1/3-octave band levels for the far-field receivers. (a) Downwind receivers, OC1, (b) upwind receivers, OC1, (c) Downwind receivers, OC2, (d) upwind receivers, OC2.

of 8.3 m/s for OC1 and 5.1 m/s for OC2. Temperature and humidity were, respectively, 5 °C and 86% for OC1 and 8 °C and 98% for OC2. The simulated conditions are summarized in Table 2.

First, the averaged sound pressure levels are calculated over the wind turbine rotation period for the three receivers and the two operating conditions. The levels are obtained in each 1/3-octave band between 50 Hz and 10 kHz. They include the contributions from the 5 modeled wind turbines. Second, auralized signals are generated for recivers SB1, SB2, and SB3. Only the turbine closest to the receivers (WT1) is included in the audio signals. It has been verified numerically that the sound contribution from the other four wind turbines is not perceivable, being the receivers close to WT1. The duration of the samples is 15 s, to match the duration of the recorded audio samples. The background noise is added to the synthetic wind turbine noise signals to allow a comparison of recorded and auralized total noise samples. The auralized signals are generated using mono rendering to match the omnidirectional microphone recordings obtained from the measurements.

As an example, Figure 5 shows the spectrogram of the auralized (top) and recorded (bottom) signals for receiver SB2 and operating conditions OC2. It can be seen that the recorded and auralized spectrograms show similar features. In particular, the amplitude modulation associated with the blade motion is visible as expected from the position of receiver SB2 close to the crosswind direction. However, the recorded signal also presents a tonal noise around 100 Hz, not seen in the auralized signal. Listening to the audio samples suggests that this tone might be due to the mechanical noise of the wind turbine which can be heard in these conditions (OC2). The 100 Hz tone was not added to the auralized signal because it was known only thanks to the measurements and, hence, it would have been an empirically-based correction added *a posteriori* to match the recorded signal. The prediction of the tonal (probably mechanical) contribution is out of the scope of the present work that focuses on aerodynamic noise emissions. If the sound power and, possibly, the directivity of the mechanical noise are provided by the manufacturer, this additional noise source can be added and the noise level at the receiver position can be calculated using the Harmonoise method.

The auralized signals include the log-amplitude fluctuations for a sound propagating in a turbulent atmosphere. The method described in reference [31] has been applied to each blade segment of each blade. For the calculation of the log-amplitude fluctuations, the source height is supposed constant and equal to the hub height. This simplification might affect the perceived noise levels because the blades move considerably in the vertical direction.

Table 3. Distance of the far-field receivers from the closest wind turbine (WT3).

Receiver	P1	P6	P8	P9	C1	C3	C5
Distance from WT3 [m]	308	933	1255	1562	331	448	744

The development of a model for the log-amplitude fluctuations that considers time-varying turbulence quantities and source height has not been developed yet. In reference [31] the same (for every frequency band) Gaussian signal w is used in the convolution with the impulse response of the log-amplitude fluctuations to obtain the time domain sequence. Here, the same Gaussian signals w are used at low frequencies ($<$800 Hz) only when the cross-frequency coherence is high ($>$0.1). At high frequencies ($\geq$800 Hz), the coherence between 1/3-octave bands is low ($\leq$0.1), and, hence, a different Gaussian signal is used for each frequency band. The calculation of the cross-frequency coherence is detailed by Ostashev et al. [32]. Even though the propagation distance is relatively small for the studied receivers, the amplitude fluctuations are audible, as demonstrated by the following audio files.

- Audio 1: Auralized noise for OC2 and SB2 without amplitude fluctuations.
- Audio 2: Auralized noise for OC2 and SB2 with amplitude fluctuations.
- Audio 3: Recorded noise for OC2 and SB2.

Significant improvement in the realism of auralized noise is observed when compared to noise signals without turbulence-induced amplitude fluctuations.

4 Validation results

This section presents the comparison of the calculated levels and auralized signals as described above with the measured data described in Section 2.

4.1 Level comparison

Figure 6 shows the averaged 1/3 octave band spectra obtained for operating conditions OC1 and OC2 for the three receivers SB1, SB2, and SB3. As shown in Figure 4, they are, approximately, in the upwind, crosswind, and downwind direction, respectively. The difference between measured and predicted 1/3-octave band levels is shown in Figure 7.

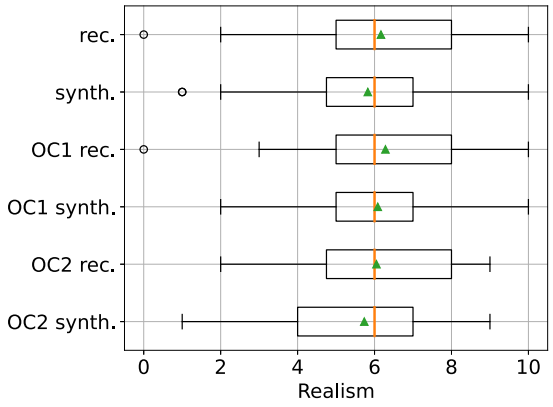
As shown in Figure 6, the numerical results accurately capture the trends of the measurements. The largest differences (Fig. 7) are observed for OC2 in the 100 Hz band due to the mechanical noise that is not modeled by the numerical simulations. Furthermore, differences up to approximately 10dB for OC1 are noticed between 2 and 5 kHz. The amplitude increase of the measured spectra could be attributed to the blunt trailing-edge noise or the tip- vortex noise (or a combination of both). These additional noise sources are not modeled in the present approach. Note that the blunt trailing-edge noise, due to the finite size of the trailing edge of the blades, is however usually absent in more recent wind turbine blade designs. The same consideration can be done for the tip-vortex noise, caused by the vortex generated at the blade tip. These additional noise sources are less evident at lower rotational speed (OC2), confirming their aerodynamic nature.

The predicted spectra for SB1 and SB3 slightly underestimate the measurements by 2-3 dB in the frequency ranges where the trailing-edge noise is the dominant noise source. This underestimation is noticeable between 250 Hz and 2000 Hz[2] and it could be explained with an underestimation of the blade loading that is used to calculate the angles of attack for the RANS simulations. Indeed, an increase in the blade loading would result in a higher induced angle of attack, and, in general, this results in higher noise levels. However, this increase would affect also the results for SB2, which have a very good match with the measured levels. For this reason, an attempt with a higher blade load has not been made and the accuracy obtained is considered within the scope of the mid-fidelity methodology developed. Furthermore, it should be recalled that the precise CAD of the turbine blade is not available and the blade of a similar turbine is used instead.

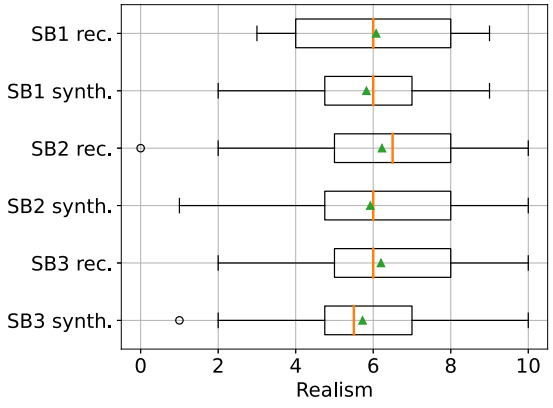
Since the receivers SB1, SB2, and SB3 were on the ground on a hard measurement board, the Harmonoise model predicts a ground attenuation of exactly 6 dB in the entire frequency range, as expected. So, the same results could be obtained in free-field conditions by adding 6 dB and the attenuation due to the atmospheric absorption. For this reason, Figure 6 cannot be used to conclude the accuracy of the Harmonoise model in predicting ground attenuation. Instead, this is done by comparing the predicted and measured spectra for the far-field microphones that are at a height above the ground between 1.45 and 1.7 m.

The accuracy of the far-field propagation model, i.e. Harmonoise, in predicting the ground attenuation is assessed for the receivers P1 to P6 and C1 to C5. This work complements the findings of [33] where a point source model was used instead. A soft ground with flow resistivity $\sigma = 500$ kPa s/m^2, which is representative of an uncompacted, loose ground, such as grass, is used in the simulation. The predicted and background-corrected measured noise spectra are shown in Figure 8. The distance of each receiver from the closest turbine (WT3) is given in Table 3 and ranges from 300 to 1500 m. These receivers are above the ground and, hence, the ground attenuation is frequency-dependent due to constructive and destructive interference of the sound waves. Only a few points are shown for the

[2] It will be shown in Section 5.1 that the trailing-edge noise is the dominant noise source above 250 Hz.



(a)



(b)

Figure 9. Perceived realism of recorded (rec.) and auralized (synth.) audio samples, considering (a) all samples (top two scores) and conditions OC1 and OC2, separately (last four scores) and (b) the SBs separately. The boxplots show the average score (green marker), the median value (orange bar), the 25–75% quartiles (black box), the statistical minimum and maximum values (black bar), and the outliers (black circles).

measured spectra because the background noise is dominant for most frequencies. However, the measured trends are visible and accurately captured by the Harmonoise model. In terms of absolute levels, a good agreement between measurements and predictions is observed for the downwind receivers, whereas the predicted noise spectra for the upwind receivers C1, C3, and C5 underestimate the measurements by 2–4 dB in the ranges where the trailing and leading-edge noises are the dominant noise sources. The reason for this slight underestimation is not clear and could be due to multiple factors, such as non-uniform ground resistivity, uncertainties in weather conditions, or an underestimation of the source spectra, as already noticed for SB1 and SB3. Furthermore, it should be remembered that the expected accuracy of the Harmonoise model is ±3 dB in the prediction of ground attenuation. As also noticed for the near-field microphones, the mechanical noise is evident in OC2 at 100 Hz.

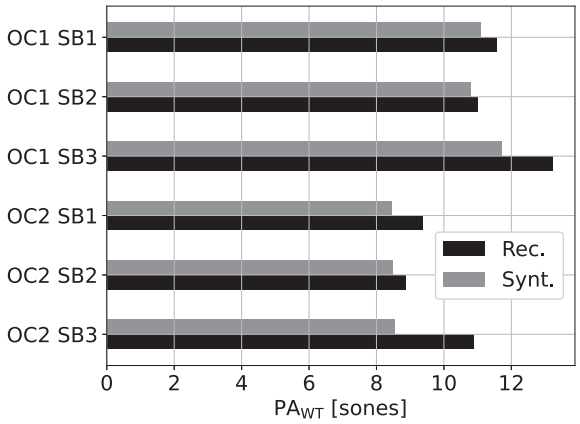
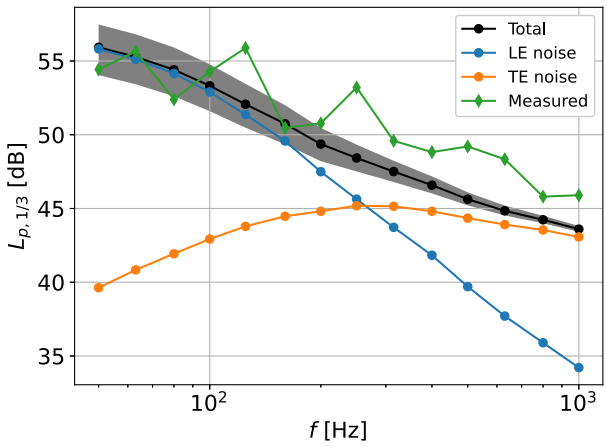


Figure 10. Averaged psychoacoustic annoyance PA_{WT} in sones.

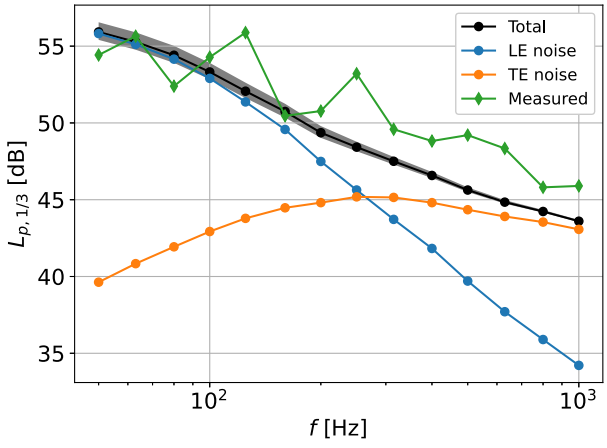
4.2 Listening tests

Listening tests were performed to evaluate the ability of the proposed auralization approach to replace in-situ audio recordings for noise annoyance studies and demonstrators. As a first result, these tests were aimed at assessing the perceived realism of the auralized audio samples. A panel of 20 subjects, none expert in the field and with no hearing problems, were asked to give a note between 0 and 10 using integer values for each of the 12 audio samples. The samples are approximately 15 s long, corresponding to 6 blade rotations. They correspond to the three receivers, SB1, SB2, and SB3, for the two operating conditions, OC1 and OC2, and the two sample types, recorded and auralized. The samples are presented in a random order, with the additional constraint of no more than 3 consecutive samples of the same type. The subject may repeat a given sample as desired but must move to the following sample once the note is given. The reproduction system includes a RME Babyface audio interface and a pair of Senheiser HD600 headphones. The system calibration was performed using a microphone placed inside the headphone cavity while positioned on a soft armrest with a 1000 Hz pure tone. While this procedure does not guarantee a precisely calibrated system, the authors believe it will not affect the listening test results since the tests compare stimuli. Also, while a wide band calibration using proper equalization would guarantee an exact frequency content, the open-type Senheiser HD600 headphones do not significantly modify the reproduced signal within the frequency range of interest. The tests are carried out in a quiet room with a measured background noise level of 31 dB(A). Before the test, the subject reads the following instruction: "You will listen to 12 audio samples of wind turbine noise of 15 s each. Imagine yourself outside in the vicinity of an operating wind turbine. For each sample, evaluate the realism with a note on a 0 (small) to 10 (large) scale. You may listen to the sample several times. You must move to the next sample once your note is given".

The audio files with the auralized and recorded noises are given below, except the ones for SB2 and OC2 that have been already presented in Section 3.



(a)



(b)

Figure 11. Effect of a 20% increase and decrease in the (a) turbulence intensity and (b) integral length scale on the predicted spectrum for SB3 and OC1.

- Audio 4: Auralized noise for OC1 and SB1.
- Audio 5: Auralized noise for OC1 and SB2.
- Audio 6: Auralized noise for OC1 and SB3.
- Audio 7: Auralized noise for OC2 and SB1.
- Audio 8: Auralized noise for OC2 and SB3.
- Audio 9: Recorded noise for OC1 and SB1.
- Audio 10: Recorded noise for OC1 and SB2.
- Audio 11: Recorded noise for OC1 and SB3.
- Audio 12: Recorded noise for OC2 and SB1.
- Audio 13: Recorded noise for OC2 and SB3.

Figure 9a presents the realism scores, shown as box and whisker plots, considering first, all receivers and operating conditions (top two scores) and second, all receivers of the same operating conditions (lower four scores). Considering all receivers and operating conditions, results show a perceived level of realism comparable to both recorded and auralized samples. The median is 6 in both cases with an average value of 6.16 and 5.83 for the recorded and auralized samples, respectively. Now looking at the two operating conditions separately, the realism scores show similar trends. The auralized samples for the higher wind conditions, OC1, yield a slightly improved averaged score than conditions, OC2, the median value remaining at 6 for all cases. The audible presence of mechanical noise which is not included in the model does not affect the realism for non-experts listeners. The spread of the perceived realism is slightly larger for the recorded samples. A possible explanation is the presence of additional noise sources, such as mechanical noise, leading to different interpretations of the associated signal features depending on the subject.

Now considering scores of realism for each receiver (Fig. 9b), the auralized samples have averaged and median values that are equal or very close to the recorded samples. Overall, it is not possible to identify a receiver or operating conditions that perform significantly better or worse than the average. Therefore, the proposed approach has the same level of realism for the three receiver positions (upwind, crosswind, and downwind) and the two sets of operating conditions.

The limitation of this study is related to the experience of the subjects. Most of them had never experienced wind turbine noise before participating in the test and, hence, it was probably difficult for them to assign a plausibility score. This is probably the reason why even recorded audio files obtained a relatively low plausibility score. In future listening tests, the subjects should be trained with recorded wind turbine noise audio files before starting the test.

4.3 Psychoacoustic annoyance

A measure of the annoyance of wind turbine sound that takes into account fluctuation strength and loudness can be derived from the model for *psychoacoustic annoyance* PA, described in [34]. As suggested in [35], the parameters for sharpness S and roughness R can be set to zero for wind turbines. Hence, the psychoacoustic annoyance of wind turbines $\mathrm{PA_{WT}}$ is defined as

$$\mathrm{PA_{WT}} = N_5(1 + w_r) \tag{5}$$

where

$$w_r = \frac{2.18}{N_5^{0.4}}(0.4F) \tag{6}$$

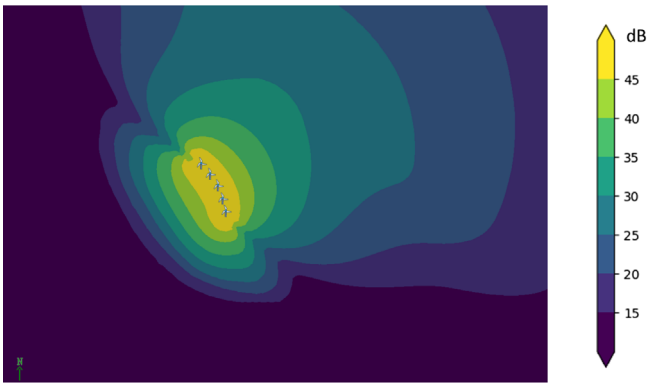
and N_5 is the loudness value exceeded for 5% of the sampling time. The loudness N is calculated using the Python package MOSQITO [36]. For broadband noise the fluctuation strength F is calculated as [34]

$$F = \frac{5.8(1.25\mu - 0.25)(0.05L - 1)}{(f_m/5)^2 + (4/f_m) + 1.5} \tag{7}$$

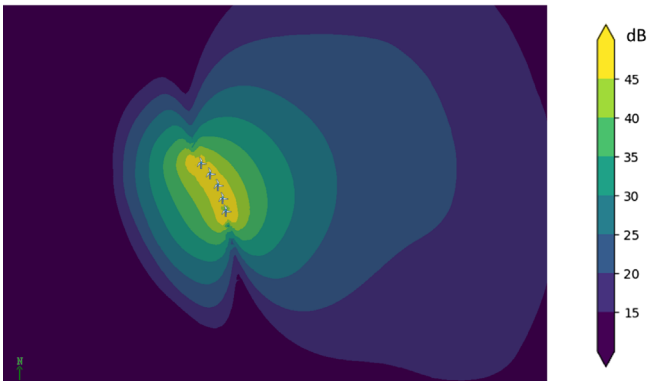
where $f_m = \mathrm{RPM}/60$ is the modulation frequency in Hz, L is the broadband noise level in decibels and μ is the modulation factor. The modulation factor μ can be computed as

$$\mu = \frac{10^{R_{mm}/20} - 1}{10^{R_{mm}/20} + 1}, \tag{8}$$

where the depth of modulation R_{mm} is calculated as $R_{\mathrm{mm}} = L_{\max} - L_{\min}$, with $L_{\max}$ and $L_{\min}$ denotes the



(a) OC1



(b) OC2

Figure 12. Predicted, overall noise levels between 63 Hz and 8 kHz, 1.5 m above the ground. The size of the computational domain is 9.3 km × 6.6 km.

maximum and minimum noise level in decibels. The averaging period is 43 ms, equivalent to 1/100 of the rotation period. The indicator PA_{WT} is calculated for the 12 audio signals used for the listening tests. This psychoacoustic annoyance metric was presented in reference [37] and has shown good performance in estimating wind turbine noise annoyance.

The resulting averaged indicators are given in Figure 10a. The auralized noise captures the trends and the values of the recorded signals, demonstrating that the auralization can be used to complement or substitute audio recordings in the evaluation of PA_{WT} . In particular, lower values of PA_{WT} are observed for OC2 due to the lower noise levels in that condition. A larger discrepancy between predicted and measured annoyance is noticed in the upwind direction (SB3), but a clear and convincing explanation has not been identified. Further studies could focus on verifying with listening tests that the indicator PA_{WT} is a relevant indicator to evaluate the annoyance of wind turbine noise, similarly to what has been done in [38].

5 Weather effects

This section analyses the effects of meteorological conditions on noise emissions and propagation by using the numerical model.

5.1 Turbulence intensity and integral length scale

The turbulence intensity and integral length scale are necessary inputs for the leading-edge (LE) noise Amiet's theory and, hence, the choice of these parameters influences the overall accuracy of the predicted spectra. In this section, we want to evaluate the relative importance of these parameters in the predicted spectra supposing a 20% increase or decrease of the reference values. Since the LE noise is mainly affecting the low-frequency range we focus on the 1/3-octave bands lower than 1000 Hz. Furthermore, we will present the results of this analysis for the near-field upwind receiver SB3 and one turbine only. Finally, the atmospheric absorption can be neglected below 1000 Hz for the near field receivers, and, so, we present the free-field results calculated with Schlinker and Amiet's theory [27][3].

Figure 11 shows the predicted spectra. The separate contributions of leading- and trailing-edge (TE) noise are also presented to quantify the relative importance of LE and TE noise. For SB3 and OC1, LE noise becomes the dominant noise source below 250 Hz. Nevertheless, the increase in the noise levels due to LE noise is visible up to 1000 Hz. The effect of the turbulence intensity variation is presented with the grey area in Figure 11a. The upper and lower limits correspond to turbulence intensities of 15.6% and 10.4%, respectively, resulting in deviations from the reference levels up to 2 dB. The maximum difference between the lower and upper limits is reached at 50 Hz and it is 3.5 dB. These deviations are consistent with the measurements presented in [39]. The deviation increases with decreasing frequency because the relative importance of LE noise increases. The integral length scale is less important (see Fig. 11b) with approximately 1 dB difference between the lower and higher limits obtained with length scales of 360 m and 240 m, respectively.

5.2 Atmospheric refraction

The refraction caused by the effective sound speed gradient influences the noise propagation by bending the sound rays towards lower sound speed regions. Simple engineering ray-based models, such as the ISO9613-2, are not able to capture this phenomenon which is instead considered by more complex numerical methods such as the Harmonoise model used in this work. The effect of the sound speed gradient on noise propagation is presented for the entire wind farm on a large computational grid of approximately 9.3 km × 6.6 km. The computational time required to generate the noise maps presented below in Mithra-SOUND® is less than one hour for each OC.

Figure 12 shows the contours of the overall noise levels of the wind farm 1.5 m above the ground for OC1 and OC2. The effect of the sound speed gradient is noticeable in the noise maps. This effect is modest within 500 m of the wind farm and it becomes more and more pronounced with increasing distance. In the upwind direction, the noise levels

[3] 6 dB are added to the free-field results to account for the hard-measurement board.

rapidly decrease because of the refraction due to the sound speed gradient that bends the sound rays upwards. This creates a shadow region, where there is no direct path between the turbine sources and the receivers. The noise emitted by the turbines can still reach this region because of the turbulence scattering effect. The Harmonoise model considers this phenomenon and it should be mentioned that the present results include the recently implemented calculation of the effective structure function parameter based on the Monin-Obukhov similarity theory [29]. As expected, the effect of the sound speed gradient is less pronounced in OC2 due to the lower wind speed. The directivity of the entire wind farm shows lower noise levels in the crosswind direction. This is due to the directivity of an isolated turbine which typically presents two main lobes in the upwind and downwind direction. Similar findings have been reported in [2] for a single wind turbine. The noise maps presented demonstrate the necessity of considering the effect of atmospheric refraction in far-field noise propagation.

6 Conclusions

This work presents the validation against field measurements of a novel workflow to predict and auralize wind turbine noise. The method is physics-based. It includes a model of the leading- and trailing-edge noise emission, coupled with the Harmonoise far-field propagation model. In addition to averaged and instantaneous sound pressure levels, the approach allows the generation of audio signals, representative of the wind turbine noise. These auralized samples can then be used to assess noise annoyance through listening tests or describe specific noise features with psychoacoustics indices.

The predicted noise spectra from five wind turbines capture well the measured trends and the absolute levels. A slight underestimation of up to 3 dB is noticed for some receivers and in the high-frequency range where the trailing-edge noise is the dominant noise source. Larger deviations from the measurements can be explained by additional noise sources not modeled in the present approach. In particular, a low-frequency tone is noticed at 100 Hz, probably due to the mechanical noise of the gearbox, and a high-frequency aerodynamic noise is identified, which might be caused by the tip-vortex of the blades and/or by their blunt trailing edge.

Next, listening tests were performed with 20 non-expert subjects to evaluate the realism of the auralized signals. No statistical evidence suggests that the auralized signals are less realistic than the recorded signals, even when considering the operating conditions and the receivers separately.

Finally, we present a study of the weather effects on noise emissions and propagation based on the numerical model developed. First, we perform a sensitivity study of the leading-edge noise model by varying the turbulence intensity and the integral length scale. It has been found that the leading-edge noise is mainly affected by variations in the turbulence intensity while it is less sensitive to variations in the integral length scale. For this reason, an, ideally, measured value of the turbulence intensity should be used for the simulations. If a measured value is not available, CFD simulations of the atmospheric boundary layer could be performed to obtain an accurate estimate. The last option is the use of the Monin–Obukhov similarity theory, for which larger errors are to be expected. Second, the effect of atmospheric refraction is evaluated for two wind speeds, confirming the findings of previous works and showing the shadow region upwind of the wind farm.

Funding

The European Commission supported this research through the H2020-MSCA-ITN-209 project zEPHYR (grant agreement No 860101). The authors also thank UMRAE for contributing to the experimental measurement campaign used in this work.

Conflict of interest

The authors declare that they have no conflicts of interest in relation to this article.

Data availability statement

This article includes selected audio files embedded in the article. The complete set of audio files for this article is available in Zenodo, under the reference [40].

References

1. S.A. Janssen, H. Vos, A.R. Eisses, E. Pedersen: A comparison between exposure response relationships for wind turbine annoyance and annoyance due to other noise sources. Journal of the Acoustical Society of America 130, 6 (2011) 3746–3753.
2. B. Cotté: Coupling of an aeroacoustic model and a parabolic equation code for long range wind turbine noise propagation. Journal of Sound and Vibration 422 (2018) 343–357.
3. Y. Tian, B. Cotté: Wind turbine noise modeling based on Amiet's theory: effects of wind shear and atmospheric turbulence. Acta Acustica united with Acustica 102, 4 (2016) 626–639.
4. Y. Tian: Modeling of wind turbine noise sources and propagation in the atmosphere. PhD thesis, Université Paris-Saclay, 2016.
5. S. Oerlemans, J.G. Schepers: Prediction of wind turbine noise and validation against experiment. International Journal of Aeroacoustics 8, 6 (2009) 555–584.
6. S. Buck, S. Oerlemans, S. Palo: Experimental validation of a wind turbine turbulent inflow noise prediction code. AIAA Journal 56 (2018) 1495–1506.
7. F. Bertagnolio, H.A. Madsen, A. Fischer: A combined aeroelastic-aeroacoustic model for wind turbine noise: verification and analysis of field measurements. Wind Energy 20, 8 (2017) 1331–1348.
8. F. Bertagnolio, T. Hansen, L.S. Søndergaard, T. Sørensen, A. Fischer, J. Feng, C. Nyborg, A. Vignaroli, K.S. Hansen, H.A. Madsen, A. Peña, W.Z. Shen, S. Oerlemans, E. Thysell, C. Volk: DecoWind: Development of low-noise and cost-effective wind farm control technology, in: Proceedings of 51st International Congress and Exposition on Noise Control Engineering – Scottish Event Campus, Glasgow, United Kingdom, 21–24 August, 2022.
9. R. Pieren, K. Heutschi, M. Müller, M. Manyoky, K. Eggenschwiler: Auralization of wind turbine noise: emission synthesis. Acta Acustica united with Acustica 100, 1 (2014) 25–33.
10. R.K. Amiet: Acoustic radiation from an airfoil in a turbulent stream. Journal of Sound and Vibration 41, 4 (1975) 407–420.
11. R.K. Amiet: Noise due to turbulent flow past a trailing edge. Journal of Sound and Vibration 47, 3 (1976) 387–393.
12. D. Mascarenhas, B. Cotté, O. Doaré: Synthesis of wind turbine trailing edge noise in free field. JASA Express Letters 2 (2022) 033601.

13. D. Mascarenhas: Physics-based synthesis of wind turbine noise. PhD Thesis, Institut Polytechnique de Paris, École nationale supérieure de techniques avancées (ENSTA), 2023.
14. J. Maillard, J. Jagla: Auralization of urban traffic noise – quantitative and perceptual validation, in: Proceedings of Congrès Français d'Acoustique (CFA), Poitiers, France, 22–25 April, 2014.
15. J. Maillard, A. Kacem: Auralization applied to the evaluation of pedestrian and bike paths in urban environments, in: Proceedings of Internoise 2016, Hamburg, Germany, August 21–24, 2016.
16. J. Maillard, A. Kacem, N. Martin, B. Faure: Physically-based auralization of railway rolling noise, in: Proceedings of the 23rd International Congress on Acoustics, Aachen, Germany, 9–13 September, 2019.
17. E. Salomons, D. Van Maercke, J. Defrance, F. De Roo: The Harmonoise sound propagation model. Acta Acustica united with Acustica 97, 1 (2011) 62–74.
18. D. van Maercke, J. Defrance: Development of an analytical model for outdoor sound propagation within the Harmonoise project. Acta Acustica united with Acustica 93 (2007) 201–212.
19. D. Ecotière, B. Kayser, B. Gauvreau, C. Lebourdat, F. Bruneau, G. Guillaume, H. Lefevre: Émission et propagation du bruit des éoliennes: constitution d'une base de données expérimentale de référence, in: Proceedings of Congrès Français d'Acoustique (CFA), Le Havre, France, 23–27 April, 2018.
20. J. Maillard, A.P.C. Bresciani, A. Finez: Perceptual validation of wind turbine noise auralization, in: Forum Acusticum 2023, Turin, Italy, 11–15 September, 2023.
21. M.J. Churchfield: A method for designing generic wind turbine models representative of real turbines and generic Siemens SWT-2.3-93 and Vestas V80 specifications. National Renewable Energy Laboratory, Golden, Colorado, 2013.
22. J. Christophe, S. Buckingham, C. Schram, S. Oerlemans: zEPHYR – large on shore wind turbine benchmark [Data set]. Zenodo, 2022. https://zenodo.org/records/7323750.
23. A.P.C. Bresciani, U. Boatto, S. Le Bras, P. Bonnet, L.D. de Santana: Influence of blade deflections on wind turbine noise directivity. Journal of Physics: Conference Series 2257 (2022) 4.
24. S. Lee: Empirical wall-pressure spectral modeling for zero and adverse pressure gradient flows. AIAA Journal 56, 5 (2018) 1818–1829.
25. M. Goody: Empirical spectral model of surface pressure fluctuations. AIAA Journal 42, 9 (2004) 1788–1794.
26. A.P.C. Bresciani, S. Le Bras, L.D. de Santana: Generalization of Amiet's theory for small reduced-frequency and nearly-critical gusts. Journal of Sound and Vibration 524 (2022) 116742.
27. R.H. Schlinker, R.K. Amiet: Helicopter rotor trailing edge noise. Technical report, National Aeronautics and Space Administration, 1981.
28. S. Sinayoko, M.J. Kingan, A. Agarwal: Trailing edge noise theory for rotating blades in uniform flow. Proceedings of the Royal Society A: Mathematical, Physical and Engineering Sciences 469, 2157 (2013) 20130065.
29. A.P.C. Bresciani, J. Maillard, S. Le Bras, L.D. de Santana: Wind turbine noise synthesis from numerical simulations, in: 29th AIAA/CEAS Aeroacoustics Conference, San Diego, CA and online, 12–16 June, 2023.
30. Weather spark. Available at https://fr.weatherspark.com (accessed 2023-04-28).
31. A.P.C. Bresciani, J. Maillard, L.D. de Santana: Physics-based scintillations for outdoor sound auralization. Journal of the Acoustical Society of America 154, 2 (2023) 1179–1190.
32. V.E. Ostashev, M.J. Kamrath, D.K. Wilson, M.J. White, C.R. Hart, A. Finn: Vertical and slanted sound propagation in the near-ground atmosphere: Coherence and distributions. Journal of the Acoustical Society of America 150 (2021) 3109–3126.
33. L. Bouma, M. Malbois, A.P.C. Bresciani, J. Maillard, S. Moreau, L.D. de Santana: Far-field propagation of wind turbine noise using the harmonoise model, in: 29th AIAA/CEAS Aeroacoustics Conference, San Diego, CA, 12–16 June, 2023.
34. H. Fastl, E. Zwicker: Psychoacoustics – facts and models, Springer, 2007.
35. C.H. Hansen, C.J. Doolan, K.L. Hansen: Measurement, in: C.H. Hansen, C.J. Doolan, K.L. Hansen (Eds.), Wind farm noise: measurement, assessment, John Wiley & Sons Ltd, 2017.
36. G.F. Coop: MOSQITO Version 1.0.8. 2022. Available at https://github.com/Eomys/MoSQITo.
37. R. Merino Martinez, R. Pieren, B. Schäffer, D.G. Simons: Psychoacoustic model for predicting wind turbine noise annoyance, in: Proceedings of the 24th International Congress on Acoustics (ICA), Gyeonju, Korea, Democratic People's Republic of, 24–28 October, 2022.
38. R. Merino-Martínez, R. Pieren, B. Schäffer: Holistic approach to wind turbine noise: from blade trailing-edge modifications to annoyance estimation. Renewable and Sustainable Energy Reviews 148 (2021) 9.
39. S. Buck, S. Oerlemans, S. Palo: Experimental characterization of turbulent inflow noise on a full-scale wind turbine. Journal of Sound and Vibration 385 (2016) 219–238.
40. A.P.C. Bresciani, J. Maillard, A. Finez: zEPHYR - Audio files of recorded and auralized wind turbine noise, Zenodo, 2024. https://doi.org/10.5281/zenodo.10657853.

Cite this article as: Bresciani APC. Maillard J. & Finez A. 2024. Wind farm noise prediction and auralization. Acta Acustica, **8**, 15.